Oh *et al.*
Journal of Analytical Science and Technology (2024) 15:31
https://doi.org/10.1186/s40543-024-00447-z

Journal of Analytical Science and Technology

RESEARCH ARTICLE Open Access

Dynamics of acyl carrier protein in de novo fatty acid synthesis by *Enterococcus faecalis* based on NMR spectroscopy and molecular dynamics simulation

Sujung Oh[1], Chaeyoung Lee[1], Minwon Son[1], Jiwon Yeon[1] and Yangmee Kim[1*]

Abstract

Fatty acid synthesis (FAS) is essential for the production of biological components such as cell membrane building blocks and metabolism-related compounds. There are two types of bacterial FAS: de novo FAS and FAS through the incorporation of external fatty acids. *Enterococcus faecalis* possesses two distinct acyl carrier proteins (ACPs), AcpA (EfAcpA) and AcpB (EfAcpB), which serve as cofactors in the two types of FAS. We previously showed through NMR spectroscopy that EfAcpA comprises only three long helices, while EfAcpB consists of four helices, including a short α_3 helix, similar to other bacterial ACPs. An increase in melting temperature (T_m) from 64.0 to 76.1 °C confirmed that protein structural stability increased in the presence of calcium ions. Using NMR spectroscopy, two metal binding sites were identified in EfAcpA: site A was located at the start of the α_2 helix while site B was situated near the α_2 helix and $\alpha_2\alpha_3$ loop. To understand the importance of structural flexibility of EfAcpA in de novo FAS, we investigated its motional properties using backbone spin relaxation and molecular dynamics simulations. The $\alpha_2\alpha_3$ loop in EfAcpA displayed high flexibility, as indicated by low heteronuclear NOE values. The residues Val51, Glu54, and Gly58 exhibited significant R_2 values, likely due to the movement of this loop. EfAcpA created a novel cavity towards the $\alpha_1\alpha_2$ loop, in contrast to conventional cavity formation in most bacterial ACPs. This unique behavior was attributed to the flexibility exhibited by the $\alpha_2\alpha_3$ loop. The structural and motional characteristics of EfAcpA confirmed that its conformational plasticity is a crucial factor influencing acyl chain transfers in de novo FAS. Given the increasing antibiotic resistance observed for *E. faecalis* in clinical settings, the findings of this study may contribute to the development of more effective pathogen management strategies targeting FAS.

Keywords Acyl carrier protein, NMR spectroscopy, Backbone dynamics, MD simulation, De novo fatty acid synthesis, *Enterococcus faecalis*

Introduction

Enterococcus faecalis, an important gram-positive bacterium commonly found in the intestines, exhibits remarkable resilience under environmental stresses, such as high temperatures, salinity, and antibiotic exposure (Kuch et al. 2012). *E. faecalis* exhibits high resistance to oxidative and dry stresses, and thrives under high salinity levels (such as 6.5% NaCl or 40% bile salts) and over a broad pH range (Orr et al. 2002; Wade 1997). Particularly noteworthy is its wide temperature tolerance: *E. faecalis* can grow at 10–40 °C and survive at 85 °C. This heat resistance enables its persistence in hospital laundry settings (Diarra et al. 2023; Laport et al. 2003). In human hosts, especially in medical settings, *E. faecalis* has been

*Correspondence:
Yangmee Kim
ymkim@konkuk.ac.kr
[1] Department of Bioscience and Biotechnology, Konkuk University, Seoul 05029, Republic of Korea

associated with life-threatening infections. Moreover, *E. faecalis* can develop resistance to various antibiotics, including vancomycin, cephalosporins, penicillin, and aminoglycosides, through genetic mutations (Hourigan et al. 2024; Nallapareddy et al. 2011; Strobel et al. 2024). Vancomycin-resistant enterococci are of special concern given their highly infectious nature in hospital settings (Eichel et al. 2023).

Fatty acids are fundamental biological components, and fatty acid synthesis (FAS) plays a vital role in the creation of cell membranes, energy storage molecules, and signaling compounds (Beld et al. 2015; Paiva et al. 2021). Additionally, fatty acids regulate post-translational protein function and can influence gene expression (Uauy et al. 2000). Bacteria typically utilize type II FAS systems, which are characterized by separate individually expressed enzymes, unlike the multifunctional complexes in eukaryotes (White et al. 2005). Acyl carrier proteins (ACPs) are key cofactors in FAS and essential for transferring acyl groups to FAS-related enzymes (Chan and Vogel 2010; Singh et al. 2023). The structures of various type II ACPs isolated from different organisms have been extensively examined. The solution structures of ACPs from *Escherichia coli*, *Bacillus subtilis*, *Mycobacterium tuberculosis*, *Vibrio harveyi*, *Helicobacter pylori*, *Borrelia burgdorferi*, and *Plasmodium falciparum* have been elucidated using NMR spectroscopy (Barnwal et al. 2011; Chan et al. 2010; Choi et al. 2021; Holak et al. 1988; Lee et al. 2020; Park et al. 2004, 2016; Sharma et al. 2006; Wong et al. 2002; Wu et al. 2009; Xu et al. 2001; Yeon et al. 2022). *E. coli* ACP (EcACP), an extensively studied bacterial ACP (Kim and Prestegard 1989; Roujeinikova et al. 2002), possesses two metal binding sites. ACPs are highly acidic proteins and divalent cations can help stabilize the electrostatic repulsion resulting from these acidic residues.

To address the emergence of antibiotic resistance in *E. faecalis*, we previously determined the solution structures of two *E. faecalis* ACPs using NMR spectroscopy. *E. faecalis* AcpA (EfAcpA) is an essential cofactor in de novo FAS, whereas *E. faecalis* AcpB (EfAcpB) is an essential cofactor in FAS using external fatty acids (Park et al. 2016; Yeon et al. 2022). We found that these two ACPs exhibited differences in the presence of the α_3 helix: EfAcpA possessed only three helices and lacked α_3, which was present in EfAcpB. These ACPs showed a low sequential identity of 28.7%, and the presence of a long $\alpha_2\alpha_3$ loop due to the lack of α_3 in EfAcpA suggested that the two ACPs serve different functions (Yeon et al. 2022).

In this study, we investigated the influence of divalent cations on the structural stability of EfAcpA and identified its metal-binding sites by measuring the melting temperature (T_m) and chemical shift perturbation (CSP) upon the addition of calcium ions. To understand the role of structural flexibility in acyl chain transfer in EfAcpA due to the absence of the α_3 helix, we explored the dynamic properties of EfAcpA using backbone spin relaxation and molecular dynamics (MD) simulations. This study aimed to elucidate the significance of structural flexibility in determining the distinct roles and functions of EfAcpA, with the ultimately goal of contributing to the development of novel antibiotics against *E. faecalis*.

Results

Comparative sequence analysis of EfAcp

To identify the key residues associated with ACP functions, we conducted sequence alignments of EfAcpA, EfAcpB, and EcACP as a reference (Fig. 1a). The majority of bacterial ACPs, including EcACP, possess a proline residue at the end of the $\alpha_2\alpha_3$ loop, only just preceding α_3. In contrast, EfAcpA has Glu54 and EfAcpB has Ser58 at this position. In EcACP, Phe28 played a key role in accessing the acyl chain, a function mirrored by Ile27 and Ile31 in EfAcpA and EfAcpB, respectively. Two residues are absent in the $\alpha_2\alpha_3$ loop of EfAcpA, a region where most bacterial ACPs typically feature a short α_3 helix. This suggests that this deletion sequence in this region facilitates the lack of α_3 in EfAcpA. All ACPs featured conserved DSL (or DSI) motifs crucial for the binding of 4′-phosphopantetheine prosthetic binding sites, along with a conserved serine at the beginning of α_2. EfAcpA harbored Leu38 and Phe39 at the beginning of α_2, which may facilitate hydrophobic interactions with acyl chains as well as FAS-related enzymes. Leu42 and Leu46 are critical residues in EcACP, with side chains that act as switches and aid in accessing the acyl group within the cavity, whereas EfAcpA has isoleucine at these positions.

The structure of EcACP comprises four helices (Kim and Prestegard 1989; Roujeinikova et al. 2007; Sztain et al. 2021; Wu et al. 2009) (Fig. 1b). The α_3 in ACPs enables the flipping of chains and transfer of the acyl chain enclosed within the hydrophobic cavity to other enzymes. This mechanism is facilitated by the flexibility inherent in α_3 (Cronan 2014; Nguyen et al. 2014). In contrast, the lack of α_3 in EfAcpA creates an atypical structure consisting only of three helices (Fig. 1b). EfAcpA participates in de novo FAS, whereas EfAcpB aids in the utilization of externally acquired fatty acids (Zhu et al. 2019). These distinct functions support the unique sequence alignment and structural features of EfAcpA, prompting further investigation into the dynamic properties associated with these differences.

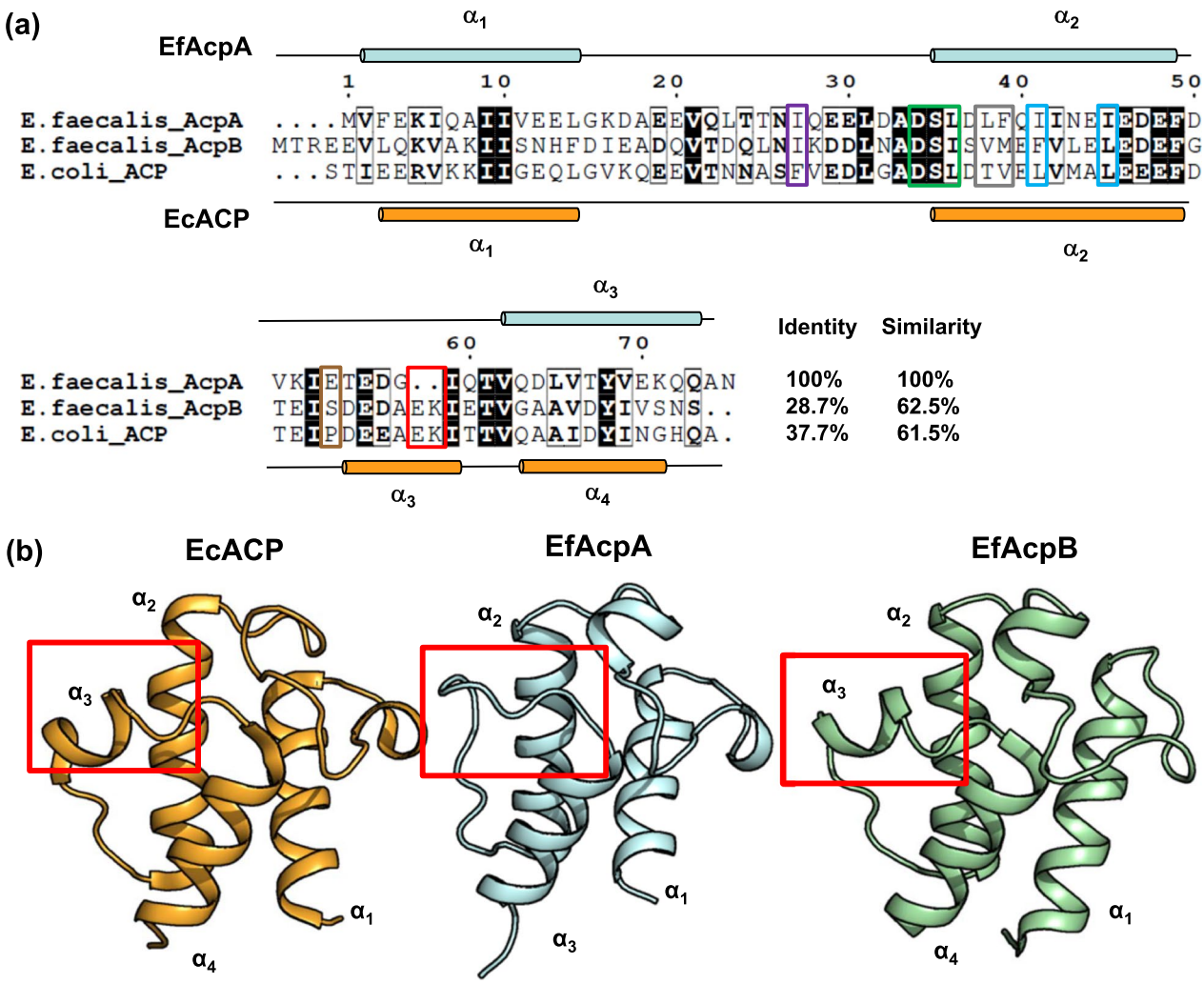

Fig. 1 Comparison of sequence and structural features of EfAcpA, EfAcpB, and EcACP. **a** The DSL motif is highlighted with a green box. Non-conserved residues, such as Ile27, are shown in purple, Leu38 and Phe39 in gray, and Glu54 in brown. Ile41 and Ile45, which correspond to Leu42 and Leu46 in EcACP and act as switches to open the subpocket in EcACP, are shown in blue. Deletion sequence in EfAcpA is marked in red. **b** Comparison of solution structures for EfAcpA (8GSA) (Yeon et al. 2022), EfAcpB (2N50) (Park et al. 2016), and EcACP (1L0I) (Roujeinikova et al. 2002)

Effect of calcium ions on the thermal stability of EfAcpA and its metal binding sites

The isoelectric point of EfAcpA was 3.7, reflecting its acidic nature associated with 21 acidic residues. The circular dichroism (CD) spectrum of EfAcpA (Fig. 2a) was examined along with the thermal denaturation curves in the range of 10–98 °C. EfAcpA displayed a typical alpha-helical structure at 25 °C in the presence of calcium as well as in the absence of calcium ion. When comparing the CD spectra of EfAcpA with and without calcium ions at 70 ℃, the protein with calcium ion exhibited a much more defined folding patterns, suggesting that calcium ions enhance the alpha-helicity of EfAcpA even at high temperature, thereby improving its structural stability. Especially, we recorded T_m of 64.0 °C in the absence of calcium and 76.1 °C in the presence of calcium, demonstrating the role of metal ions in enhancing the structural stability of EfAcpA.

We investigated the metal binding sites of EfAcpA based on the CSP in the ^{1}H-^{15}N heteronuclear single quantum coherence (HSQC) spectra during the titration of calcium ions. Superimposition of the HSQC spectra during titration revealed noticeable shifts in the HSQC peaks for specific residues, indicating the presence of potential metal-binding sites. Residues associated with > 0.13 ppm CSPs near the N-terminal of α_2 included Glu30, Asp32, Ala33, Asp34 and Ser35 (Site A, Fig. 2b). Asp47, Ile 53, Glu54, and Glu56 near the C-terminal of α_2 and the $\alpha_2\alpha_3$ loop (Site B) exhibited significant CSPs, suggesting the existence of two metal binding sites. Residues

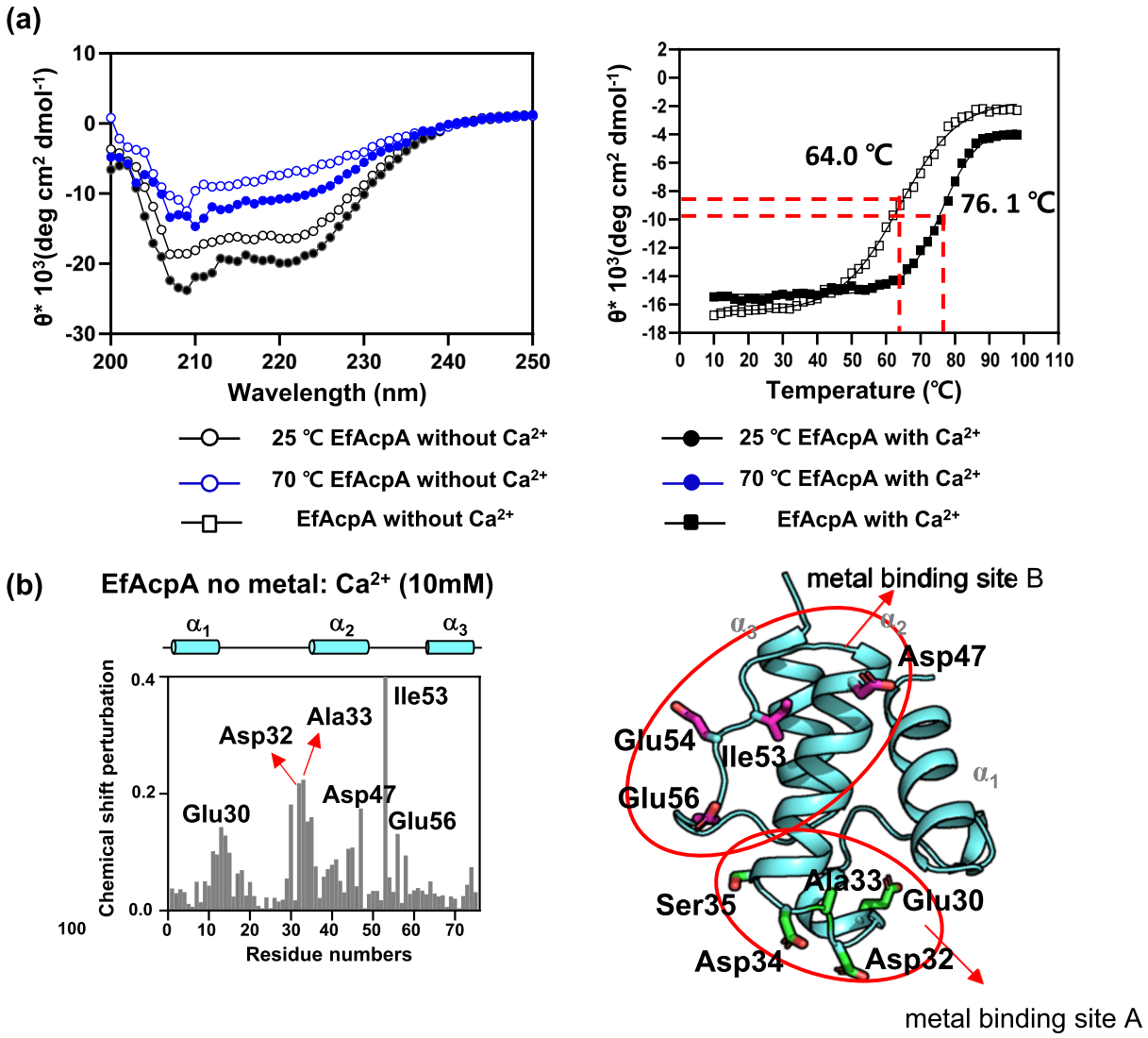

Fig. 2 Thermal stability and metal binding sites of EfAcpA. **a** Secondary structures at 25 ℃ and 70 ℃ and melting temperatures of EfAcpA in the presence and absence of calcium ion. **b** Chemical shift perturbation in ^{1}H-^{15}N HSQC spectra upon titration of EfAcpA with calcium ions from 1:0 to 1:10 ratio **c** Trace of residue peaks in ^{1}H-^{15}N HSQC spectra when EfAcpA is titrated with calcium ions in the following ratios: 1:0 (red), 1:0.5 (orange), 1:1 (yellow), 1:2 (green), 1:5 (blue), 1:10 (purple), 1:50 (pink), and 1:100 (gray)

affected by metal binding (CSP > 0.13 ppm) are mapped onto the EfAcpA structure in Fig. 2b. Figure 2c illustrates the $^{1}H–^{15}N$ HSQC peak traces of crucial residues in EfAcpA, including Glu30, Asp34, Asp47, and Glu56, during titration of calcium ions. The peaks exhibited gradual directional shifts until reaching saturation.

Backbone dynamics of EfAcpA

To elucidate the functional properties of EfAcpA, we investigated its backbone dynamics in the holo-form attached to the prosthetic group. We conducted longitudinal relaxation rate (R_1), transverse relaxation rate (R_2), and heteronuclear NOE (hNOE) experiments at picosecond to nanosecond timescales. The average rates in EfAcpA were 1.89 ± 0.02 for R_1, 8.02 ± 0.07 for R_2, and 0.79 ± 0.01 s^{-1} for hNOE (Fig. 3). The relaxation rates were comparable in stable helix regions, whereas those in the N- and C-terminal and $\alpha_2\alpha_3$ loop regions varied. The absence of a short third helix in EfAcpA generated only three helices and a long $\alpha_2\alpha_3$ loop, resulting in high flexibility in the $\alpha_2\alpha_3$ loop and low hNOE values of 0.61 ± 0.01 s^{-1} (0.18 s^{-1} lower than the average). Val51, Glu54, and Gly58 in the $\alpha_2\alpha_3$ loop exhibited higher R_2 values than other residues, suggesting that they may be crucial for shuttling acyl groups.

We compared the backbone dynamics of EfAcpA with that previously reported for EfAcpB (Park et al. 2016). Ser58 at the beginning of α_3 in EfAcpB exhibited extremely high R_2 values (39.86 ± 1.04 s^{-1}) (Park et al. 2016). In contrast, Glu54 in EfAcpA had a much lower R_2 value (9.65 ± 0.01 s^{-1}) than that of Ser58 in EfAcpB. Generally, EfAcpA did not display high conformational exchange; however, its $\alpha_2\alpha_3$ loop exhibited high structural flexibility, as evidenced by the low hNOE values.

MD simulations of EfAcpA

We performed 800 ns MD simulations of two EfAcpA replicates to investigate the role of the $\alpha_2\alpha_3$ loop in the cavity formation of EfAcpA. In EfAcpA, 4′-phosphopantetheine predominantly occupied cavity 1 due to the motion of the $\alpha_2\alpha_3$ loop (Fig. 4a). Cavity 1 was formed by Leu38, Ile42 in α_2, Ile53, Thr55 in the $\alpha_2\alpha_3$ loop, and Leu65, Val69 in α_3. While most type II bacterial ACPs possess one cavity, formed by the α_2, α_3, and $\alpha_2\alpha_3$ loop, EfAcpA exhibited a novel cavity 2 in the direction of the $\alpha_1\alpha_2$ loop. The entrance of cavity 2 was delineated by Ile27 in the $\alpha_1\alpha_2$ loop and Leu38 in α_2. Cavity 2 was formed by Ile6, Ile10, and Leu14 in α_1; Thr25, Ile27, Leu31 in the $\alpha_1\alpha_2$ loop; Leu38, Ile41 in α_2 and Val62 in α_3. When the distance between Ile27 C_α and Leu38 C_α increased, cavity 2 opened up (the red circled area in Fig. 4b). However, entry seemed to be hindered by the short length of 4′-phosphopantetheine. The distance

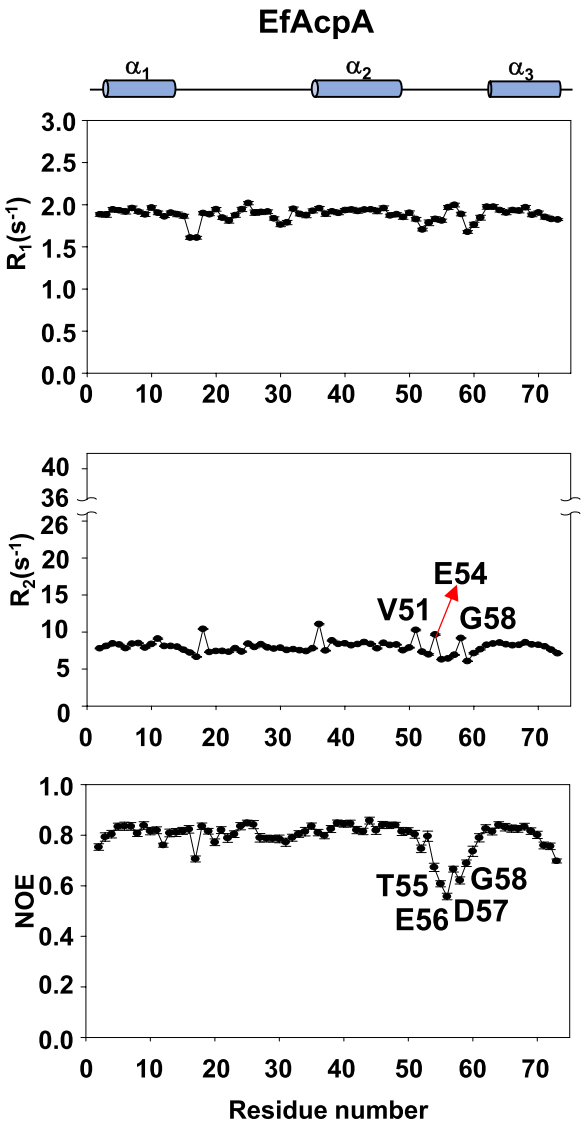

Fig. 3 Spin relaxation rates of EfAcpA. R_1, R_2, and hNOE values for EfAcpA were measured at 298 K. The values are plotted in relation to the residue sequence number for EfAcpA, the bars above the plots indicate the helices of EfAcpA

between Ile27 C_α and Leu38 C_α remained constant otherwise, indicating that 4′-phosphopantetheine primarily resided in cavity 1. Consistent with the hNOE values observed in the backbone dynamics analysis, the root mean square fluctuations (RMSF) estimated for both EfAcpA replicates demonstrated that the $\alpha_2\alpha_3$ loop was highly flexible (Fig. 4c). Based on the MD simulations of EfAcpA, the highly flexible $\alpha_2\alpha_3$ loop did not facilitate the stable formation of the entrance to cavity 1, leading to the continuous shuttling of 4′-phosphopantetheine (Fig. 4d).

We also conducted MD simulations to investigate the effect of calcium ions in stabilizing the structure of

EfAcpA. The calcium ions binding near two metal binding sites of EfAcpA resulted in the stabilization of the flexible $\alpha_2\alpha_3$ loop, as depicted in Fig. 4e.

Discussion

ACPs are small acidic proteins comprising four helices and three loops. ACPs sequester acyl chains in a cavity to facilitate their transfer to other enzymes while preventing their hydrolysis. However, EfAcpA possesses a distinctive structure and cavity characterized by only three helices and two loops. Therefore, we explored the structural flexibility of EfAcpA and the effect of divalent cations on the stability of EfAcpA using CD and NMR spectroscopy as well as MD simulations.

The T_m and metal binding site experiments showed that the presence of calcium ions increased thermal stability by 12.1 degree. Similarly, the T_m of EfAcpB and EcACP increased in the presence of calcium ions (EfAcpB: 72.5 °C → 78.8 °C, EcACP: 55.0 °C → 67.2 °C) (Park et al. 2016), highlighting the importance of metals in the structural stability of ACPs. *V. harveyi* ACP exhibited protein unfolding at a neutral pH in the absence of divalent metal ions, which was attributed to strong electrostatic repulsion and a lack of histidine residues (Chan et al. 2010). Similarly, calcium ions bound to the two metal-binding sites of EfAcpA enhanced its structural and thermal stability.

Most mesophilic ACPs typically feature a rigid proline residue at the beginning of α_3 (Fig. 1a). In contrast, EfAcpA contains a negatively charged glutamine residue, and EfAcpB features a polar serine residue with relatively short polar hydroxymethyl side chains. Previous backbone dynamics studies on EcACP revealed reported uniform R_2 and hNOE values at the beginning of α_3 due to the proline providing a rigid structure, while Ser58 of EfAcpB displayed exceptionally high R_2 rates (Park et al. 2016). These findings imply that EfAcpB undergoes faster exchanges in α_3 compared to the canonical EfAcpA, enabling the generation of various conformations for the swinging motion of the 4′-phosphopantetheine arm and shuttling of long exogeneous acyl chains.

The backbone spin relaxation and MD simulation experiments on EfAcpA demonstrated the flexibility of the $\alpha_2\alpha_3$ loop. This flexibility prevents the formation of a stable entrance to cavity 1, which leads to its collapse. Consequently, cavity 2 was formed with a more stable entrance structure. Two subpockets have been identified in EcACP accommodating the hexanoyl acyl chain (Chan et al. 2008). Subpockets 1 and 2 in EcACP share the same entrance but are situated at different positions (Fig. 5). Subpocket 1, commonly observed in the NMR and crystal structures of acyl-EcACPs, comprises α_2, α_3, and the $\alpha_2\alpha_3$ loop, whereas subpocket 2 is closer to α_1 than subpocket 1. However, the cavities of EfAcpA do not share a common entrance; instead, they form separate cavities that facilitate stable accommodation of acyl chains.

In the EcACP, Leu42 and Leu46 act as switches that allow entry to the hexanoyl acyl chain (Chan et al. 2008). However, in contrast to EcACP, Ile41 and Ile45 in EfAcpA, corresponding to Leu42 and Leu46 in EcACP, do not appear to serve as switches. Furthermore, the cavities in EfAcpA were positioned differently. The flexibility of the $\alpha_2\alpha_3$ loop in EfAcpA plays a role in forming a new cavity 2, contributing to a distinctive cavity structure in EfAcpA.

Conclusions

We elucidated the structural stability and flexibility of EfAcpA, an essential cofactor in de novo FAS by *E. faecalis*. We identified two metal binding sites of EfAcpA in the presence of calcium ions along with enhanced thermal stability facilitated by reduced electrostatic repulsion, particularly in the region surrounding the elongated and flexible long $\alpha_2\alpha_3$ loop. Unlike most bacterial ACPs, EfAcpA lacks a short helix and is characterized by high flexibility in the $\alpha_2\alpha_3$ loop and the formation of the unique cavity 2. These structural features may play a role in interacting with FAS-related enzymes and the shuttling of acyl chains. Further research is required to understand potential correlations and underlying mechanisms. Our findings provide valuable insights into the mechanism by which EfAcpA facilitates acyl chain transfer in de novo FAS.

Methods

Expression and purification of EfAcpA

The *acpA* gene from *E. faecalis* was cloned into the pET-28a vector. After converting the recombinant vector into *E. coli* BL21 (DE3), the cells were grown in 500 mL M9 minimal medium with $^{15}NH_4Cl$ to express EfAcpA.

(See figure on next page.)

Fig. 4 MD simulations on EfAcpA. **a** Representative illustration of cavities 1 and 2 within EfAcpA. **b** Distance between Ile27 C_α in the $\alpha_1\alpha_2$ loop and Leu38 C_α in α_2. **c** Root mean square fluctuation (RMSF) for two EfAcpA replicates. **d** Snapshot showing the motion of Ile27, Leu38 forming the entrance to cavity 2 and the $\alpha_2\alpha_3$ loop in 800 ns. At 122.2 ns, the entrance to cavity2 was briefly opened, but 4′-phosphopantentein was unable to enter and remained primarily within cavity 1. **e** Snapshot showing the calcium binding site and demonstrating that the movement of the $\alpha_2\alpha_3$ loop is stabilized by calcium ions. The yellow spheres represent calcium ions

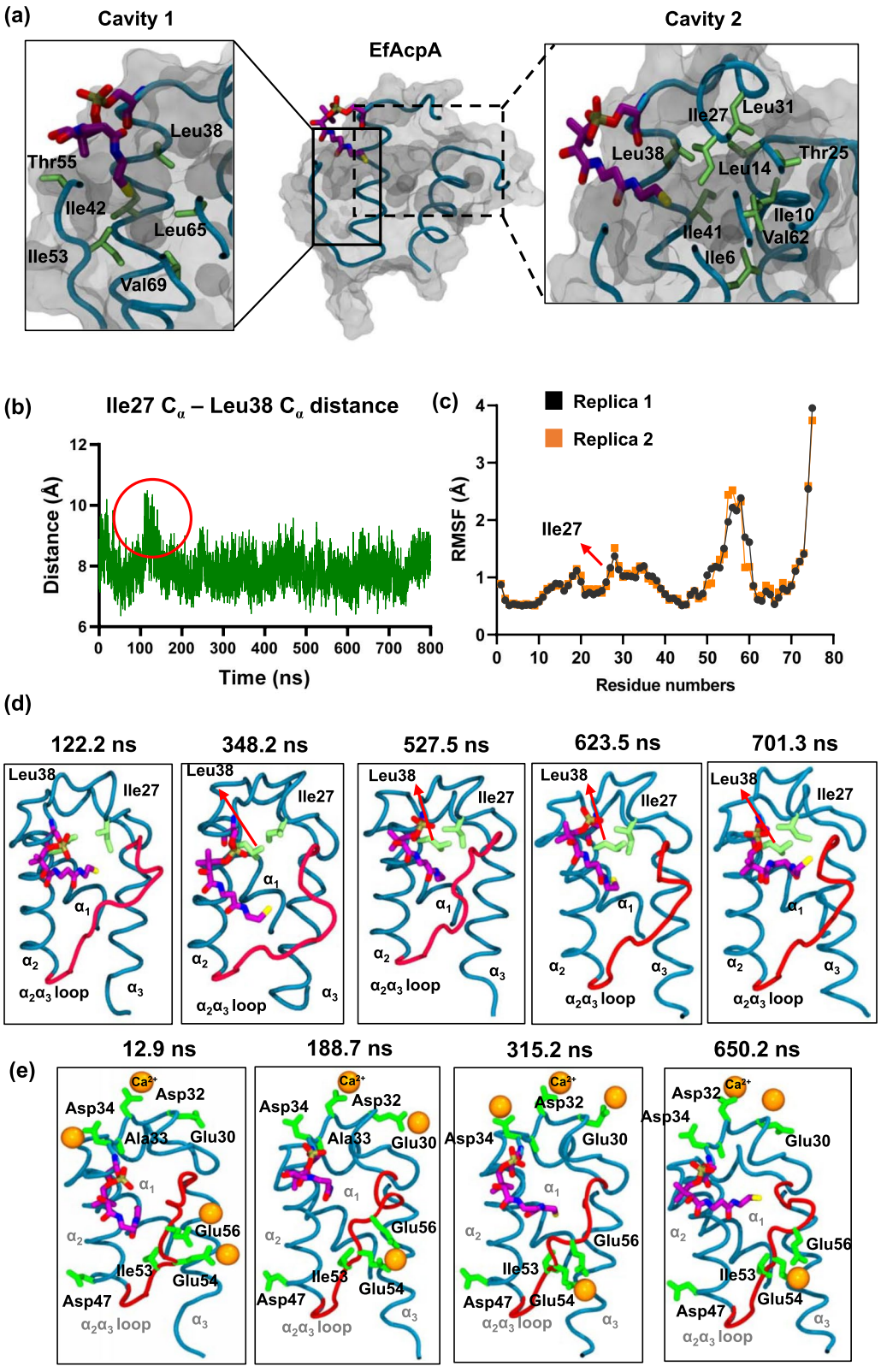

Fig. 4 (See legend on previous page.)

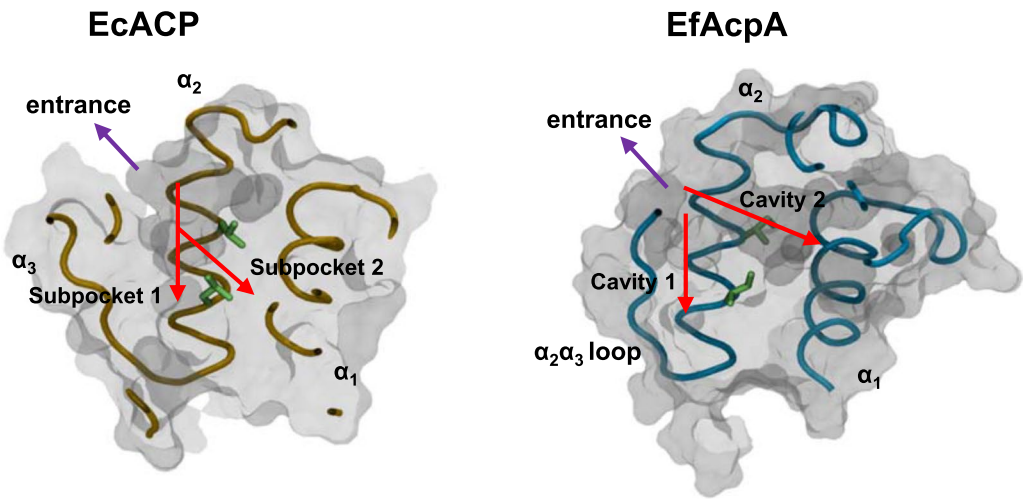

Fig. 5 Comparison of cavities in EcACP and EfAcpA. Cavities 1 and 2 are highlighted with red arrows

EfAcpA was purified as previously described (Yeon et al. 2022; Yoo et al. 2024). To produce holo-EfAcpA, apo-EfAcpA, coenzyme A, and holo-ACP synthase, *E. coli* was added and reacted at 25 °C for 16 h, and the final purification was done with HiTrap Q FF (GE Healthcare).

Detecting CSPs upon calcium ion (Ca^{2+}) titration

We identified the metal binding sites of EfAcpA through CSP analysis of ^{1}H-^{15}N HSQC spectra detected during calcium ion titration (Choi et al. 2021). This experiment was performed using a 700 MHz Bruker Avance spectrometer at the Korea Basic Science Institute (Ochang, Korea). EfAcpA samples were prepared in a buffer containing 25 mM 2-(*N*-morpholino)ethanesulfonic acid (MES), 5 mM dithiothreitol (DTT), 10% D_2O, and 0.02% NaN3 (pH 6.1). HSQC spectra were acquired by the successive addition of calcium ions at 0 mM, 0.5 mM, 1 mM, 2 mM, 5 mM, 10 mM, 50 mM, and 100 mM.

CD experiment to measure the melting temperatures of EfAcpA

We assessed the thermal stability of EfAcpA by measuring its T_m using a J1500 spectropolarimeter (Jasco, Tokyo, Japan). CD spectra were recorded from 200 to 250 nm from 10 to 98 °C, with 0.1 nm intervals, and accumulation was repeated three times. The CD spectra showed the average residual ellipticity (θ) in degrees (cm^2 $dmol^{-1}$). EfAcpA samples (50 μM) were prepared in 25 mM MES, 5 mM DTT and 25 mM MES, or 5 mM DTT, with and without 5 mM $CaCl_2$. The T_m was calculated from the CD spectra at a wavelength of 222 nm to determine the midpoint between the lowest and highest θ values.

Spin relaxation experiments

We estimated the R_1, R_2, and hNOE values of each backbone amide proton in EfAcpA using the Bruker Avance spectrometer. R_1 rates were obtained from the decay of peak heights in the HSQC spectra over 10 relaxation delays of 0.01 (×2), 0.05, 0.1, 0.2, 0.3 (×2), 0.5, 0.8 and 1.2 s. The R_2 rates were determined from 10 relaxation delays at 0 (×2), 0.01696, 0.03392, 0.05088 (×2), 0.0848, 0.13568, 0.22048 and 0.32224 s. The recycle delays were 2.3 s and 2.0 s in the R_1 and R_2 experiments, respectively. The hNOE values were obtained from the ratios of the peak heights of the interleaving pulse sequences with and without proton saturation. The recycle delay and proton-saturation pulse were 4.0 s and 3.0 s, respectively.

MD simulations

We utilized the previously reported structure of EfAcpA (8GSA) to perform MD simulations and examine the dynamics of the $\alpha_2\alpha_3$ loop. Using the Ligand Reader & Modeler tool in CHARMM-GUI, we computed the bonding of 4′-phosphopantetheine groups to serine residues. This involved the integration of acetylated N-termini (ACE) and methyl-amidated C-termini (CT3) with parameters configured according to the CGENFF protocol (version interface 1.0.0, force field 3.0.1) (Jo et al. 2008; Vanommeslaeghe et al. 2010; Yu et al. 2012). The holo-EfAcpA system was prepared using the solution builder in CHARMM-GUI by incorporating 0.15 M KCl or 0.01 M calcium ions into the TIP3P water cube model (Lee et al. 2016). We performed MD simulations with a CHARMM36m force field using OpenMM (version 7.7.0). Equilibration was performed in six consecutive steps using CHARMM-GUI under the NPT ensemble

for 1.25 s. The simulations were performed at a constant temperature of 310.15 K and isotropic pressure of 1 bar for 800 ns.

Abbreviations

ACP	Acyl carrier protein
CSP	Chemical shift perturbation
EcACP	*Escherichia coli* ACP
EfAcpA	*Enterococcus faecalis* AcpA
EfAcpB	*E. faecalis* AcpB
FAS	Fatty acid synthesis
hNOE	Heteronuclear NOE
HSQC	Heteronuclear single quantum coherence
MD	Molecular dynamics
R_1	Longitudinal relaxation rates
R_2	Transverse relaxation rates
RMSF	Root mean square fluctuation
T_m	Melting temperature

Acknowledgements
The authors would like to thank the Korea Basic Science Institute (KBSI) for technical support for the 700 MHz NMR experiments.

Author contributions
SO performed the data collection and analysis, visualization, and writing—original draft; CL performed the investigation and data curation; MS performed the investigation and data curation; JY performed the investigation, data analysis, and data curation; YK contributed to conceptualization, writing—review and editing, supervision and funding acquisition; All authors have read and approved the final version of the manuscript.

Funding
This work was supported by a National Research Foundation of Korea (NRF) grant funded by the Korean government (MSIT) [Grant Number RS-2023-00207959].

Availability of data and materials
All data generated or analyzed during this study are included in this published article. Further information can be shared upon reasonable request to the corresponding author.

Declarations

Competing interests
The authors declare that they have no competing interests.

Received: 10 May 2024 Accepted: 21 May 2024
Published online: 28 May 2024

References

Barnwal RP, Van Voorhis WC, Varani G. NMR structure of an acyl-carrier protein from *Borrelia burgdorferi*. Acta Crystallogr Sect F Struct Biol Cryst Commun. 2011. https://doi.org/10.1107/S1744309111004386.

Beld J, Lee DJ, Burkart MD. Fatty acid biosynthesis revisited: structure elucidation and metabolic engineering. Mol BioSyst. 2015. https://doi.org/10.1039/C4MB00443D.

Chan DI, Vogel HJ. Current understanding of fatty acid biosynthesis and the acyl carrier protein. Biochem J. 2010. https://doi.org/10.1042/BJ20100462.

Chan DI, Stockner T, Tieleman DP, Vogel HJ. Molecular dynamics simulations of the Apo-, Holo-, and acyl-forms of *Escherichia coli* acyl carrier protein. J Biol Chem. 2008. https://doi.org/10.1074/jbc.M805323200.

Chan DI, Chu BC, Lau CK, Hunter HN, Byers DM, Vogel HJ. NMR solution structure and biophysical characterization of *Vibrio harveyi* acyl carrier protein A75H: effects of divalent metal ions. J Biol Chem. 2010. https://doi.org/10.1074/jbc.M110.128298.

Choi S, Park J, Yeon J, Jang A, Lee WC, Kim Y. Deciphering the binding interactions between *Acinetobacter baumannii* ACP and β-ketoacyl ACP synthase III to improve antibiotic targeting using NMR spectroscopy. Int J Mol Sci. 2021. https://doi.org/10.3390/ijms22073317.

Cronan JE. The chain-flipping mechanism of ACP (acyl carrier protein)-dependent enzymes appears universal. Biochem J. 2014. https://doi.org/10.1042/BJ20140239.

Diarra C, Goetz C, Gagnon M, Roy D, Jean J. Biofilm formation by heat-resistant dairy bacteria: multispecies biofilm model under static and dynamic conditions. Appl Environ Microbiol. 2023. https://doi.org/10.1128/aem.00713-23.

Eichel VM, Last K, Brühwasser C, von Baum H, Dettenkofer M, Götting T, et al. Epidemiology and outcomes of vancomycin-resistant *Enterococcus* infections: a systematic review and meta-analysis. J Hosp Infect. 2023. https://doi.org/10.1016/j.jhin.2023.09.008.

Holak T, Kearsley S, Kim Y, Prestegard J. Three-dimensional structure of acyl carrier protein determined by NMR pseudoenergy and distance geometry calculations. Biochemistry. 1988. https://doi.org/10.1021/bi00416a046.

Hourigan D, Stefanovic E, Hill C, Ross RP. Promiscuous, persistent and problematic: insights into current enterococcal genomics to guide therapeutic strategy. BMC Microbiol. 2024. https://doi.org/10.1186/s12866-024-03243-2.

Jo S, Kim T, Iyer VG, Im W. CHARMM-GUI: a web-based graphical user interface for CHARMM. J Comput Chem. 2008. https://doi.org/10.1002/jcc.20945.

Kim Y, Prestegard J. A dynamic model for the structure of acyl carrier protein in solution. Biochemistry. 1989. https://doi.org/10.1021/bi00448a017.

Kuch A, Willems RJ, Werner G, Coque TM, Hammerum AM, Sundsfjord A, et al. Insight into antimicrobial susceptibility and population structure of contemporary human *Enterococcus faecalis* isolates from Europe. J Antimicrob Chemother. 2012. https://doi.org/10.1093/jac/dkr544.

Laport MS, Da Silva MR, Silva CC, do Carmo-de-Freire-Bastos M, Giambiagi-de-Marval M. Heat-resistance and heat-shock response in the nosocomial pathogen *Enterococcus faecium*. Curr Microbiol. 2003. https://doi.org/10.1007/s00284-002-3828-0.

Lee J, Cheng X, Jo S, MacKerell AD, Klauda JB, Im W. CHARMM-GUI input generator for NAMD, GROMACS, AMBER, OpenMM, and CHARMM/OpenMM simulations using the CHARMM36 additive force field. J Chem Theory Comput. 2016. https://doi.org/10.1021/acs.jctc.5b00935.

Lee Y, Jang A, Jeong MC, Park N, Park J, Lee WC, et al. Structural characterization of an ACP from *Thermotoga maritima*: Insights into hyperthermal adaptation. Int J Mol Sci. 2020. https://doi.org/10.3390/ijms21072600.

Nallapareddy SR, Singh KV, Sillanpää J, Zhao M, Murray BE. Relative contributions of Ebp Pili and the collagen adhesin ace to host extracellular matrix protein adherence and experimental urinary tract infection by *Enterococcus faecalis* OG1RF. Infect Immun. 2011. https://doi.org/10.1128/iai.00038-11.

Nguyen C, Haushalter RW, Lee DJ, Markwick PR, Bruegger J, Caldara-Festin G, et al. Trapping the dynamic acyl carrier protein in fatty acid biosynthesis. Nature. 2014. https://doi.org/10.1038/nature12810.

Orr K, Holliday M, Jones A, Robson I, Perry J. Survival of enterococci during hospital laundry processing. J Hosp Infect. 2002. https://doi.org/10.1053/jhin.2001.1137.

Paiva P, Medina FE, Viegas M, Ferreira P, Neves RP, Sousa JP, et al. Animal fatty acid synthase: a chemical nanofactory. Chem Rev. 2021. https://doi.org/10.1021/acs.chemrev.1c00147.

Park SJ, Kim J-S, Son W-S, Lee BJ. pH-induced conformational transition of *H. pylori* acyl carrier protein: insight into the unfolding of local structure. J Biochem. 2004. https://doi.org/10.1093/jb/mvh041.

Park Y-G, Jung M-C, Song H, Jeong K-W, Bang E, Hwang G-S, et al. Novel structural components contribute to the high thermal stability of acyl carrier protein from *Enterococcus faecalis*. J Biol Chem. 2016. https://doi.org/10.1074/jbc.M115.674408.

Roujeinikova A, Baldock C, Simon WJ, Gilroy J, Baker PJ, Stuitje AR, et al. X-ray crystallographic studies on butyryl-ACP reveal flexibility of the structure around a putative acyl chain binding site. Structure. 2002. https://doi.org/10.1016/s0969-2126(02)00775-x.

Roujeinikova A, Simon WJ, Gilroy J, Rice DW, Rafferty JB, Slabas AR. Structural studies of fatty acyl-(acyl carrier protein) thioesters reveal a hydrophobic binding cavity that can expand to fit longer substrates. J Mol Biol. 2007. https://doi.org/10.1016/j.jmb.2006.09.049.

Sharma AK, Sharma SK, Surolia A, Surolia N, Sarma SP. Solution structures of conformationally equilibrium forms of holo-acyl carrier protein (PfACP) from *Plasmodium falciparum* provides insight into the mechanism of activation of ACPs. Biochemistry. 2006. https://doi.org/10.1021/bi060368u.

Singh K, Bunzel G, Graf B, Yip KM, Neumann-Schaal M, Stark H, et al. Reconstruction of a fatty acid synthesis cycle from acyl carrier protein and cofactor structural snapshots. Cell. 2023. https://doi.org/10.1016/j.cell.2023.10.009.

Strobel AG, Prasad P, Prasad V, Naidu R, Young-Sharma T, Suka A, et al. The epidemiology of *enterococci* in a tertiary hospital and primary healthcare facilities in Fiji (2019–2022). J Glob Antimicrob Resist. 2024. https://doi.org/10.1016/j.jgar.2024.03.008.

Sztain T, Bartholow TG, Lee DJ, Casalino L, Mitchell A, Young MA, et al. Decoding allosteric regulation by the acyl carrier protein. Proc Natl Acad Sci U S A. 2021. https://doi.org/10.1073/pnas.2025597118.

Uauy R, Mena P, Rojas C. Essential fatty acids in early life: structural and functional role. Proc Nutr Soc. 2000. https://doi.org/10.1017/S00296651000000021.

Vanommeslaeghe K, Hatcher E, Acharya C, Kundu S, Zhong S, Shim J, et al. CHARMM general force field: A force field for drug-like molecules compatible with the CHARMM all-atom additive biological force fields. J Comput Chem. 2010. https://doi.org/10.1002/jcc.21367.

Wade J. *Enterococcus faecium* in hospitals. Eur J Clin Microbiol Infect Dis. 1997. https://doi.org/10.1007/BF01709469.

White SW, Zheng J, Zhang Y-M, Rock CO. The structural biology of type II fatty acid biosynthesis. Annu Rev Biochem. 2005. https://doi.org/10.1146/annurev.biochem.74.082803.133524.

Wong HC, Liu G, Zhang Y-M, Rock CO, Zheng J. The solution structure of acyl carrier protein from *Mycobacterium tuberculosis*. J Biol Chem. 2002. https://doi.org/10.1074/jbc.M112300200.

Wu BN, Zhang YM, Rock CO, Zheng JJ. Structural modification of acyl carrier protein by butyryl group. Protein Sci. 2009. https://doi.org/10.1002/pro.11.

Xu G-Y, Tam A, Lin L, Hixon J, Fritz CC, Powers R. Solution structure of *B. subtilis* acyl carrier protein. Structure. 2001. https://doi.org/10.1016/S0969-2126(01)00586-X.

Yeon J, Oh S, Hwang E, Kim E, Kim Y. Structural study of acyl carrier protein of *Enterococcus faecalis* and its interaction with enzymes in de novo fatty acid synthesis. Biochem Biophys Res Commun. 2022. https://doi.org/10.1016/j.bbrc.2022.11.023.

Yoo S, Yeon J, Kim E, Kim Y. Important features for protein foldings in two acyl carrier proteins from *Enterococcus faecalis*. J Microbiol Biotechnol. 2024. https://doi.org/10.4014/jmb.2309.09006.

Yu W, He X, Vanommeslaeghe K, MacKerell AD Jr. Extension of the CHARMM general force field to sulfonyl-containing compounds and its utility in biomolecular simulations. J Comput Chem. 2012. https://doi.org/10.1002/jcc.23067.

Zhu L, Zou Q, Cao X, Cronan JE. *Enterococcus faecalis* encodes an atypical auxiliary acyl carrier protein required for efficient regulation of fatty acid synthesis by exogenous fatty acids. Mbio. 2019. https://doi.org/10.1128/mbio.00577-19.

Publisher's Note